Feature identification using acoustic signature of Ocean Researcher III of Taiwan

Y.-Y. Fang[1] C.-F. Chen[2] S.-J. Wu[3]

17 November 2017; revised 18 February 2019

Abstract

Underwater acoustic signature identification has been employed as a technique for detecting underwater vehicles, such as in anti-submarine warfare or harbour security systems. The underwater sound channel, however, has interference due to spatial variations in topography or sea state conditions and temporal variations in water column properties, which cause multipath and scattering in acoustic propagation. Thus, acoustic data quality control can be very challenging. One of challenges for an identification system is how to recognise the same target signature from measurements under different temporal and spatial settings. This paper deals with the above challenges by establishing an identification system composed of feature extraction, classification algorithms, and feature selection with two approaches to recognise the target signature of underwater radiated noise from a research vessel, Ocean Researcher

DOI:10.21914/anziamj.v59i0.12655, Published July 25, 2019, as part of the Proceedings of the 13th Biennial Engineering Mathematics and Applications Conference. ISSN 1445-8810. (Print two pages per sheet of paper.)

III, with a bottom mounted hydrophone in five cruises in 2016 and 2017. The fundamental frequency and its power spectral density are known as significant features for classification. In feature extraction, we extract the features before deciding which is more significant from the two aforementioned features. The first approach utilises Polynomial Regression (PR) classifiers and feature selection by Taguchi method and analysis of variance under a different combination of factors and levels. The second approach utilises Radial Basis Function Neural Network (RBFNN) selecting the optimised parameters of classifier via genetic algorithm. The real-time classifier of PR model is robust and superior to the RBFNN model in this paper. This suggests that the Automatic Identification System for Vehicles using Acoustic Signature developed here can be carried out by utilising harmonic frequency features extracted from unmasking the frequency bandwidth for ship noises and proves that feature extraction is appropriate for our targets.

Subject class: 03C45

Keywords: feature identification; acoustic signature; Taguchi method; ANOVA; ship noise; passive acoustic monitoring

Contents

1 Introduction

Underwater acoustic signature identification has been employed as a technique for detecting underwater vehicles, such as in anti-submarine warfare or harbour security systems. Passive Acoustic Monitoring (PAM) uses hydrophones for detecting underwater targets, monitoring underwater habitats over a long time period [1, 2], or observing underwater seismic activity [3].

Applying underwater acoustic signature identification for analysing the massive data from PAM is quicker and easier to use than experienced human operators (EHO). There are different strategies to enhance the detection accuracy. First, regarding signal processing and noise reduction [4], Wang enhanced the target signal by Hilbert-Huang transform [5]. Weiss also applied a noise reduction and reconstruction technique to high-frequency acoustic signals by wavelet transforms [6]. Second, utilising feature extraction to increase identification, Bodisco focused on selecting key features from an electroglottograph signal by Markov-chain Monte Carlo statistical modelling [7]. Third, regarding classification algorithms, Ribeiro-Fonseca used artificial intelligence as a classifier to increase the recognition rate of ship noise [8].

Data quality control also is challenging, with problems of ambient noise by time/space-varying multipaths arising when the underwater acoustic propagation is influenced by ever-changing sound speed profiles under different topography or sea state conditions [4, 9]. The biggest noise masking issue is shipping noise masking, as it is a continuous low-frequency anthropogenic sound [10, 11], but its acoustic signatures are valuable features in anti-submarine warfare or harbour security systems. Therefore, this research project used the target signature of underwater radiated noise from a research vessel, Ocean Researcher III (OR3), with a bottom mounted hydrophones in five cruises between 2016 to 2017. There are two groups in the data set classified by EHO. One is the "OR3" (called Target 1, T=1), and the other is "Non-OR3" (called Target 0, T=0), which includes the ambient noise with other ship noises, such as cargo ships, naval vessels, fishing boats.

The goal of this study is to identify the two opposing acoustic signatures from data of different cruises and how to extract the significant features from time/space-varying target signals (which show that the signal to noise ratio is unstable in each cruise) for use in the classifier, thereby automatically identifying the correct target.

Three steps are employed, composed of feature extraction, classification algorithms, and feature selection, in two approaches for an Automatic Identi-

fication System for Vehicles using Acoustic Signature (AIS4VAS) compare the identification (refer to Figure 1) and verify the diagnostic ability via receiver operating characteristic (ROC) [12, 13, 14], the coefficient of determination (R^2) [15], and correlation coefficient (R).

The process of feature extraction in the two approaches is the same and compares frequency or power spectral density (PSD), which are significant in feature extraction. The fundamental frequency (FF) is an inherit property of the type of the ship and independent of specific time and location of the ship, but it can be masked by ambient noise because both ship noise and much of the ambient noise are louder in lower frequencies. The problem is how to extract FF from the noise masking problem. The process extracts the "same" FF, which is called "Main Frequency" (MF); its harmonic frequency (HF); and sound pressure level (SPL) from different cruising data. We define Occurrence Frequency (OF) and HF from FF, and we present a new definition by combining Occurrence Times of OF (OT) and Harmonic Times of HF in OF (HT) when extracting MF. Then, SNR (signal to noise ratio) is utilised to solve the noise masking problem and quantify the original signal corruption and meaningful information, which includes combinations of MF, its PSD, and the interaction of these two terms.

The first approach essentially is curve fitting by the Polynomial Regression (PR) classifiers to approximate the SNR of the collected data, and statistically analysed using the Taguchi method and ANOVA, and facilitate our feature extraction. The major difference, is that unlike the standard statistical (polynomial) regression, is that our classifier is constructed from two complementary surrogate models (OR3 and Non-OR3). We desire to enhance the prediction based on the accuracy and sensitivity of each models (Table 2). To reduce the combination of building classifiers from full factor design to factorial design, we apply the Taguchi method to feature selection, which could increase the computational efficiency and find the optimal combination of the controllable factors (Table 3).

The Taguchi method is a cost-driven quality engineering method providing

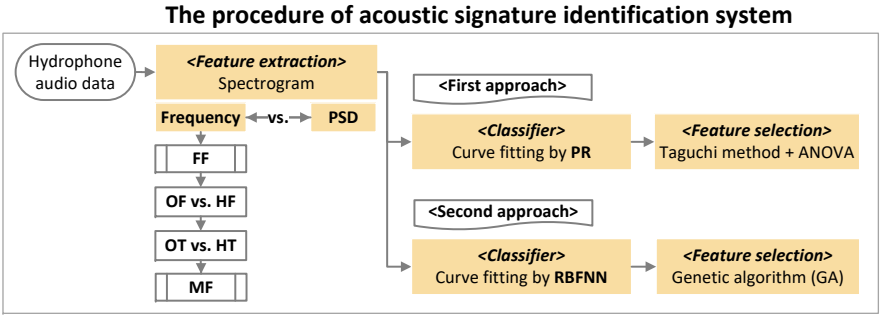

Figure 1: Flow chart of Automatic Identification System for Vehicles using Acoustic Signature (AIS4VAS). (PSD: Power spectral density; FF: Fundamental frequency; MF: Main frequency; OF: Occurrence frequency; HF: Harmonic frequency in occurrence frequency; OT: Occurrence Times of occurrence frequency; HT: Harmonic Times of harmonic frequency in occurrence frequency; PR: Polynomial Regression; ANOVA: Analysis of variance; RBFNN: Radial Basis FunctionăNeural Network)

optimisation for factorial design to cut the cost and number of experiments by using orthogonal arrays [16, 17, 18, 20]. Orthogonal arrays are constructed with a fraction of a full factorial array to save exhaustive testing of every possible input to the system. It is orthogonal between the factors, and the factors are independent from each other and in balance (Figure A.1). A reduced model, made from a general linear model [21], for evaluating classifiers under the optimal arrangements of versatile models' factors was analysed using the Taguchi method and analysis of variance (ANOVA).

The second approach is curve fitting by Radial Basis Function Neural Network (RBFNN) [22, 23] and feature selection by genetic algorithm (GA) [24] to find the optimising parameters of the classifier. The neural network is a processing system in artificial intelligence that mimics a biological neural network, using artificial neurons (consisting of processing units and nodes) for parallel computing. The advantages are that it has strong curve-fitting operations for nonlinear models, its model has good prediction, and has been

performed in many areas of signal processing. This study utilises RBFNN, which consists of a hidden layer of a nonlinear transfer function-radial basis function network (RBF) and a linear output layer. Since the neural network learns by adjusting the weighting value and the bias in each iteration, the setting of the training parameter will affect the performance of network. Therefore, this approach of this study is combined with the GA to find the global optimum training parameters.

We developed this AIS4VAS, which extracts the essential features of the acoustic signature, utilises factor analysis in feature selection, and builds the classifier by two approaches. Then, we compare the performance with PR and RBFNN [25, 26].

2 Data acquisition

From December 2016 to August 2017, we completed six sets of field experiments on the southwestern coast of Taiwan, as seen in Table 1 and Fang [27, 28]. The whole audio data came from the radiated noise of OR3 ship noise, including idle testing (500 revolutions per minute (rpm) of main engine) and cruising speed testing (600 to 800 rpm) by bottom mounted PAM. The procedure of measurement of underwater sound from ships was according to the standards of Det Norske Veritas (DNV) Part 6 Chapter 24- Silent class notation for ships [29], the International Organisation for Standardisation (ISO) 17208-1: Acoustics- Part1 [30], and Bureau Veritas (BV) Underwater Radiated Noise (URN) rule note 614 [31].

From Table 1, the first to fifth voyages recorded the OR3 signatures under idling, cruising, and optimisation idling tests. At a minimum, the line track cruising test required two runs for either port or starboard aspect measurement under different engine operation conditions, and the test course configuration refers to ISO 17208-1 [30] and Figure 2(A). The line track was from K1 to K2, and M1 was the hydrophone location. The distance from a source to

Table 1: Introduction of data sources and experimental locations (Introduction of data samples (each dataset: 3 mins)).

Voyage	Date	Location (Taiwan)	OR3 (T=1)		Non-OR3(T=0)
			Idle	Cruise	PAM
1	2016/12/26	Changhua offshore	18	39	67
2	2016/12/27	Kaohsiung offshore	25	33	0
3	2017/04/06-04/10	Kaohsiung harbour	206	0	0
4	2017/06/05	Liuqiu offshore	5	39	5
	2017/06/05	Kaohsiung harbour	25	0	0
5	2017/08/02 - 08/15	Miaoli offshore (PAM)	0	0	318
Total number			390		390

hydrophone was between 150 and 200 meters, which is called the closest point of approach (CPA), but we adjusted the CPA to 700 meters for the experiment performed on December 27^{th}, 2017 due to high marine traffic rate in order to avoid collisions with other seas at sea. The bottom-anchored hydrophones deployment, the range of CPA, and the minimum depth under vessel followed DNV rules [29] and ISO 17208-1 [30] (Figure 2(B)).

As data acquisition was difficult from ocean experiments, the total number of OR3 targets was 390 and each sample set contains 3-minute data length. The other 318 samples of Non-OR3 were collected from a bottom mounted PAM hydrophones offshore near Miaoli from August 2 to 15 in 2017, which also extracted 3-minutes of data from each hour. The Non-OR3 samples included the ambient noise and ship noises of outboard, skiff, yacht, trawler, fishing boat, patrol boat, cargo boat, for example. The recording quality of Non-OR3 samples had no limitation of CPA and no cruising track configuration, but the hydrophone deployment still followed DNV rules.

All signatures were collected via Wildlife Acoustics instruments: Song Meter Ultrasonic autonomous submersible marine recorders (types: SM2M and SM3M) with hydrophone sensitivity (-164.5 dB re 1V/1μ Pa) and gain (0 dB).

Figure 3 shows the typical acoustic signatures of ship noise from line track

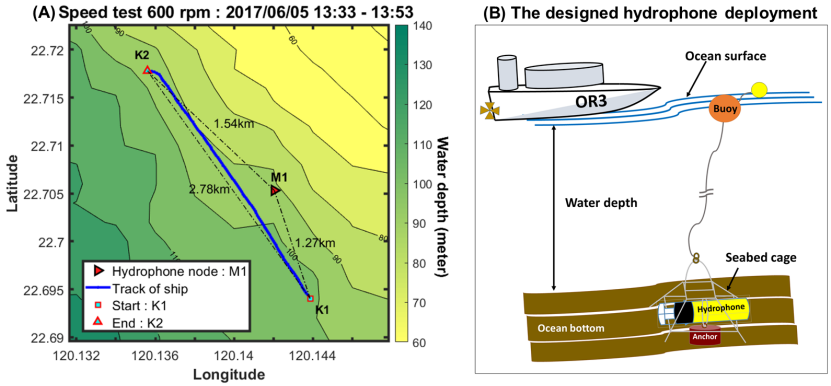

Figure 2: (A) Geographical position of the study area (Liuqiu offshore, Taiwan), with acoustic station indicated; (B) The designed hydrophone deployment of field experiments.

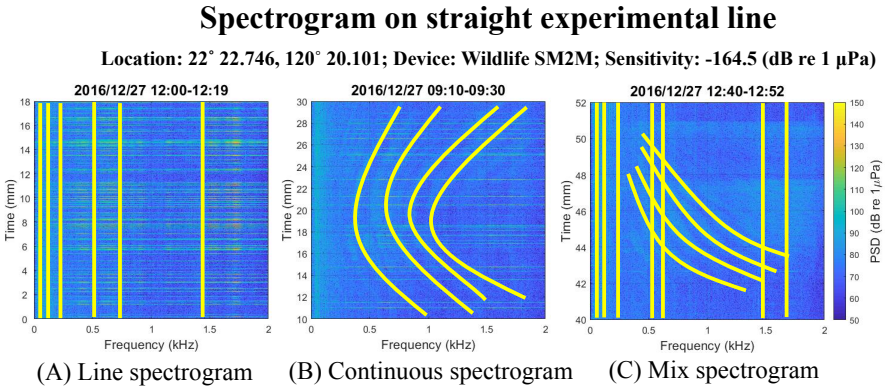

Figure 3: The three typical types of acoustic signatures from ship noise (The spectrogram is from line track cruising on 27 December 2016)

cruising on 27 December 2016. The three typical signatures from ship noise, called mixed spectrogram, consist of line spectrograms and continuous spectrograms [32]. Line spectrograms are usually caused by mechanical noise or propeller blade tones, and its harmonic tone comes from the resonance of the propeller under low speed. Continuous spectrograms are connected with a different firing rate of the engine and the blade rate of the propeller under high speeds. The mixed spectrogram will be affected by the rotational speed of mechanisms and variations of loading the propeller for different sea states. Therefore, the feature extraction of this paper will illustrate how to extract FF by slot-pole noise, fire rate, and blade rate; HF and PSD.

3 Feature extraction

In the procedure of feature extraction, the first step is to extract FF from acoustic signatures. The second step is to extract the "same" FF which is called "Main Frequency" (MF); its HF; and sound pressure level (SPL) from different cruising data. In this procedure, there are newly defined terms, explained as follows.

We used the Short Time Fourier Transform (STFT) [8] to get the spectrum information. The acoustic pressure was calculated using a 1-s Hamming window with 10% overlap under 48k sample rate (fs) for each 3-minute data set. Second, we smoothed the instantaneous noise peak by Exponential Moving Average (EMA) [33] and Gaussian smoothing filter [34]. Moreover, we only extracted the peak pressure value ($\hat{\mathbf{P}}$) from 95% of total energy. Filtering the low frequency and high frequency noise for each minute of data results in the filtering pressure value.

The frequency index of selecting 95% peaks under each bandwidth (BW) was set as the FF (as $\hat{\mathbf{F}}$). It is extracted from 3-minute data under seven BWs. The frequency range of each BW was BW1 (10-49 Hz), BW2 (50-99 Hz), BW3 (100-249 Hz), BW4 (250-499 Hz), BW5 (500-749 Hz), BW6 (750-999 Hz),

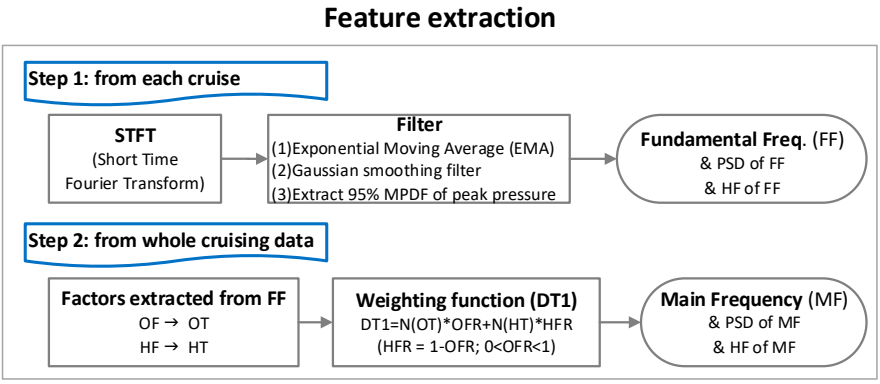

Figure 4: Flow chart of feature extraction.(MPDF: Marginal Probability Density Function; OF: Occurrence frequency; HF: Harmonic frequency in occurrence frequency;OT: Occurrence Times; HT: Harmonic Times; DT_1: Detecting Threshold one; OFR: Occurrence Frequency Ratio; HFR: Harmonic Frequency Ratio; N: normalised)

and BW7 (1000-2000 Hz) which refers to the x axes of Figure 7, Figure A.1 and Figure A.2.

New definitions in this paper are Occurrence Frequency (OF) and Harmonic Frequency (HF). The occurrence frequency ($\hat{F}_O$) and HF ($\hat{F}_H$) both belong to FF ($\hat{F}$) and are a positive integers.

Other new definitions are OT (Occurrence Times of OF) and HT (Harmonic Times of HF in OF). OT is the number of times that OF repeatedly occurs within a set of data of a 3-minute time frame with each being obtained under different conditions. We remark that OT may not be the same at different occasions; hence, a repetition of signals is seen as a universal characteristic frequency that will be addressed in the following paragraph. HT is the number of times that HF appears in OF.

$$\hat{F}_O, \hat{F}_H \in \hat{F} \quad \& \quad \hat{F}_H \in \sigma_F \cdot \hat{F}_O, \text{where} \quad \sigma_F \in Z^+. \tag{1}$$

In order to extract the acoustic signature for a particular type of ship, we will

repeatedly extract signature frequencies within a set of 3-min data, acquired at different occasions. This can be referred to as occurrence frequencies (OFs). The signature frequencies within each 3-min data is termed as occurrence frequencies (OFs). Each of these OFs will be weighted throughout the set of all 3-min data, where the weight is the number of occurrences of each OF across all datasets, which is termed as OT here. Hence, we can infer a certain OF to be the acoustic signature of the ship when its associated OT is high and vice-versa. This leads to HT, which is the number of instances that HF appears in OF.

The total number of OR3 target data is 390 sets from Table 1. We randomly chose 33 from the 332 (OR3 and Non-OR3 samples) to be a training sample, and we repeated the probability of selection until the total number of samples reached 101 sets ($\widehat{\mathsf{n}}$=101). We followed the above procedure to get OT and HT from each set. Examples of calculating the OT and HT and their correlation are in Appendix A.2.

To compare what is significant in feature extraction, we present a new definition by combining OT and HT, which is a weighting function (DT_1) in this paper. DT_1 is a kind of threshold to determine the ratio of OT and HT when extracting MF from FF.

$$\begin{aligned} &\mathsf{DT}_1(\mathsf{OT},\mathsf{HT},\mathsf{OFR}) = \mathsf{N}(\mathsf{OT})\cdot\mathsf{OFR} + \mathsf{N}(\mathsf{HT})\cdot\mathsf{HFR}, \\ &\text{where}\quad \mathsf{HFR} = 1-\mathsf{OFR}; \mathsf{OFR}(\mathsf{L}) = \begin{cases} 1, \mathsf{L}=1, \\ 0.5, \mathsf{L}=2, \\ 0, \mathsf{L}=3, \end{cases} \end{aligned} \tag{2}$$

where L is the level of the factor in Table 3. In this weighting function, we define OFR (Occurrence Frequency Ratio) and HFR (Harmonic Frequency Ratio) as weighting values for the ratio of OT to HT. These weighting values of OFR will be the first controllable factors in curve fitting (refer to Table 3), and they compare three different occasions under OFR=1 (only observe the effect of OT), OFR=0 (only observe the effect of HT), or OFR = 0.5 (observe the interaction of half OT and HT).

The second controllable factor (refer to Table 3) is defined as "Threshold" (DT_2), and its setting value is $0 < DT_2 < DT_1$. DT_2 is like the second filter, which removes the frequency that does not exceed the threshold of the weighting function ($\mathbf{DT_1}$), which is

$$\begin{aligned} \mathbf{DT_1} &= [DT_{1,1}, DT_{1,2}, ..., DT_{1,q}] = \{DT_{1,q} | DT_{1,q} \geqslant DT_2, q \leqslant w\}, \\ \text{where} \quad DT_2(L) &= \begin{cases} 0, L = 1, \\ \text{mean}(\mathbf{DT_1}), L = 2, \\ \text{median}(\mathbf{DT_1}), L = 3, \end{cases} \end{aligned} \tag{3}$$

where q is index number of $\mathbf{DT_1}$ and w is the index number of $\hat{\mathbf{F}}$ and $\hat{\mathbf{P}}$ (refer to Equation (A.3) and Equation (A.4)). After filtering by DT_2, the remaining frequency as the main frequency (MF, $\widetilde{\mathbf{F}}$)

$$MF = \widetilde{\mathbf{F}} = [\hat{F}_1, \hat{F}_2, ..., \hat{F}_q] = \{\hat{F}_q | DT_{1,q} \geqslant DT_2, q \leqslant w\}. \tag{4}$$

Thus, we can get the power spectrum density (PSD) of MF at different BWs.

$$PSD = 20 \cdot \log(\hat{P}/P_{ref}) + \text{Sensitivity} + \text{Gain}, \tag{5}$$

where $P_{ref} = 1\mu P_a$. Calculating the sensitivity of hydrophone and the gain of amplifier setting values in Equation (5) will remove the effect from instruments.

After extracting MF from the aforementioned 101 sets of OR3 target and 101 sets of Non-OR3 target, the third controllable factor (Table 3) is SNR (signal to noise ratio), which is the input samples of PR and RBFNN. Signal to Noise Ratio (SNR) is the following mathematical formula used in statistics to find the meaningful information of training samples. The meaningful information is included with MF, PSD of MF, and the interaction of these two terms.

$$\begin{aligned} &SNR = 10 \cdot \log_{10}(\tfrac{\mu^2}{\sigma^2}), \\ &\text{where} \quad SNR(L) = \begin{cases} SNR(MF), L = 1, \\ SNR(PSD), L = 2, \\ SNR(MF) \cdot SNR(PSD), L = 3, \end{cases} \end{aligned} \tag{6}$$

where μ is the mean and σ is the standard deviation of MF or PSD under different levels.

4 First approach: Polynomial Regression (PR)

Our first approach essentially was using the PR classifiers and feature selection by Taguchi method and ANOVA under different combinations of factors and levels (Table 3).

4.1 Classifier

Before curve fitting, we scaled **SNR** and utilised the unity-based normalisation as Equation (A.1). The PR classifiers were curve fitting the aforementioned $\mathbf{Z}_{\mathtt{data}} = \mathsf{N}(\mathbf{SNR})$ (Z plane) by the least square method (the derivatives are mentioned in Appendix B.1) and are

$$\hat{\mathbf{Z}} = \mathbf{X}^{\mathtt{d}} \cdot \boldsymbol{\beta} \cdot \mathbf{Y}^{\mathtt{r}} + \hat{\boldsymbol{\varphi}}, \quad \text{where} \quad \mathtt{d} = 0, 1, 2, ..., \mathsf{O}_{\mathsf{X}\Lambda}, \quad \mathtt{r} = 0, 1, 2, ..., \mathsf{O}_{\mathsf{YZ}}, \tag{7}$$

$$\hat{\boldsymbol{\varphi}} = \mathbf{Z}_{\mathtt{data}} - \hat{\mathbf{Z}}. \tag{8}$$

The X plane is a matrix from one to seven BWs, where $\boldsymbol{\beta}$ is the matrix of coefficient estimates for a multilinear regression on X plane, $\mathtt{d}$ is the setting value of power of building X plane and also the controllable factors "E" from Table 3. The Y matrix consists of the controllable factors "D" from Table 3, along with the training set size (101 in this paper), where $\mathtt{r}$ is the setting value of power from YZ plane. Equation (8) is the residual, which is the observed deducted from the predicted value. To minimise the residual as a optimising procedure of the classifier, we need to set a threshold of tolerance of error, which is called "DT_3" in this paper, following the detection decision

Table 2: A confusion matrix of receiver operating characteristic (ROC)

	T=1 (OR3)	T=0 (Non-OR3)
$\hat{\mathsf{T}}_{\mathrm{pr}}$=1 (OR3)	True Positive	False Positive
	TP = P($\hat{\mathsf{T}}_{\mathrm{pr}}$=1 ∩T=1)	FP = P($\hat{\mathsf{T}}_{\mathrm{pr}}$=1 ∩T=0)
$\hat{\mathsf{T}}_{\mathrm{pr}}$=0 (Non-OR3)	False negative	True Negative
	FN = P($\hat{\mathsf{T}}_{\mathrm{pr}}$=0 ∩T=1)	TN = P($\hat{\mathsf{T}}_{\mathrm{pr}}$=0 ∩T=0)
Accuracy (ACC) = (TN+TP)/(TN+TP+FN+FP)		

Table 3: Combinations of controllable factors and levels for Taguchi $L_{27}(3_{13})$ design.

Factor	Description	Level 1	Level 2	Level 3
A	OFR (weighting of DT_1)	1	0.5	0
B	DT2 (threshold of DT_1)	0	mean(DT_1)	median(DT_1)
C	Regression input	SNR(MF)	SNR(PSD)	SNR(MF)·SNR(PSD)
D	O_{YZ} (the power of $\mathbf{Y}^{\mathrm{r}}$)	5	4	3
E	$\mathsf{O}_{\mathsf{X}\Lambda}$ (the power of $\mathbf{X}^{\mathrm{d}}$)	6	5	4

(Equation(9)) to obtain the target value from model $\hat{\mathsf{T}}_{\mathrm{pr}}$ (one is OR3 and zero is Non-OR3). The detection decision ($\widetilde{\mathsf{f}}(\hat{\boldsymbol{\varphi}}, \mathsf{DT}_3)$)

$$\hat{\mathsf{T}}_{\mathrm{pr}} = \widetilde{\mathsf{f}}(\hat{\boldsymbol{\varphi}}, \mathsf{DT}_3) = \begin{cases} 1, & \hat{\mathsf{T}} \in \mathrm{OR3}, \quad \hat{\boldsymbol{\varphi}} \leqslant \mathsf{DT}_3, \\ 0, & \hat{\mathsf{T}} \in \text{Non-OR3}, \quad \hat{\boldsymbol{\varphi}} > \mathsf{DT}_3, \end{cases} \tag{9}$$
$$\text{where} \quad 0 \leqslant \mathsf{DT}_3 \leqslant 0.5 \quad \text{and} \quad 0 \leqslant \hat{\boldsymbol{\varphi}} \leqslant 1.$$

After getting the $\hat{\mathsf{T}}_{\mathrm{pr}}$ from the 101 samples, we utilised receiver operating characteristic (ROC) to verify the performance of the two opposite models by PR. From ROC, calculating the probability of true positive (TN), true negative (TP), false negative (FN), and false positive (FP) by the targets from the model ($\hat{\mathsf{T}}_{\mathrm{pr}}$) and from the observation (T), then the accuracy (ACC) is obtained from Table 2.

In Table 3, Factor A compares the significance of OT, HT, or both; B is a threshold of feature extraction; C compares the significance of frequency, pressure, or both; and D and E are the parameters of building the "classifier".

If we consider the whole combination of Table 3, we need to build 243 classifiers. To increase the computational efficiency and optimise the parameter design, we applied Taguchi method on feature selection in the next subsection.

4.2 Feature selection

We utilised $L_{27}(3^{13})$ OrthogoShort Time Fourier Transformnal Array (Appendix B.2: Figure B.1), which was composed of five controllable factors with three levels (Table 3). The original combination of Table 3 is 243, and the final one is only 27 through $L_{27}(3^{13})$.

The quality characteristic of Taguchi method in this paper utilised the detection accuracy of classifier (ACC) and belonged to a larger-the-best characteristic of Taguchi specified situation [16]. The formula of S/N_{LTB} is not like SNR from Equation (6) and is given as

$$S/N_{LTB} = -10 \cdot \log_{10}[\frac{1}{p}\sum_{jj=1}^{p}\frac{1}{ACC_{jj}^2}], \tag{10}$$

where p is the index number of training samples as Equation (10), jj is the index number of ACC, and ACC is calculated from Table 2.

This study used ANOVA to identify the significant controllable factors by analysing the main effect and the interaction of factors. The ANOVA results are presented in Table 4. The sum of squares (SS) is a tool to determine which of those five factors is insignificant. Since the SS of Factor B and the interaction of Factors A and B were much smaller than the others, we pulled those two terms. DOF is degrees of freedom. MS is mean square or called variance, which is calculated by SS/DOF. F value is given by MS/MS_E, which determines which variance is significantly different from others. MS_E is the variance of the error and is 0.089 from Table 4. $F_{0.05}$ is F statistic in ANOVA testing and is built on the critical value at 0.05 of F-test. If the F value was larger than $F_{0.05}$, we rejected the null hypothesis and the factor was

Table 4: ANOVA of S/N for the $L_{27}(3^{13})$ design in Table 3.

Factors	SS	DOF	MS	F_{-test}	$F_{0.05}$	P_{value}	SS'	Contribution(%)
A	4.687	2	2.343	26.409	5.143	0.001	4.509	13.67%
B	(0.050)	(2)	-	-	-	-	-	-
C	3.085	2	1.543	17.384	5.143	0.003	2.908	8.82%
D	2.802	2	1.401	15.791	5.143	0.004	2.625	7.96%
E	4.154	2	2.077	23.405	5.143	0.001	3.976	12.06%
AxB	(0.483)	(4)	-	-	-	-	-	-
AxC	1.670	4	0.418	4.706	4.534	0.046	1.316	3.99%
AxD	6.487	4	1.622	18.277	4.534	0.002	6.133	18.60%
AxE	9.559	4	2.390	26.932	4.534	0.001	9.204	27.91%
Error	0.532	6	0.089				2.307	7.00%
Total	32.978	26	*Note: At least 95% confidence				32.978	100.00%

statistically significant. The p-value is a probability that is calculated from an F-distribution with *DOF*. Pure sum of squares (SS') deducts the effect of error term from *SS*. The confidence interval (*CI*) of the estimated value with 95% confidence level is calculated by the t-distribution.

$$\mathrm{CI} = \mathrm{t}_{\hat{\alpha}/2}(\mathrm{df}_{\mathrm{E}})\sqrt{\frac{\mathrm{MS}_e}{\mathrm{n}_e}} \tag{11}$$

where df_{E} is the degree of freedom of the error, which is 6; n_e is the effective sampling number; and $\hat{\alpha}$ is the significance level, which is 0.05. After applying Equation (11), CI is 0.421 dB.

The ANOVA showed that the significant interactions were "A and E," "A and D," and "A and C," which also were shown in Figure 5. From Figure 5(A), there were two optimal combinations, which were $\mathrm{A_1E_1}$ or $\mathrm{A_3E_2}$. Following those combinations and referring to Figure 5 (B) and (C), we obtained $\mathrm{A_1C_3D_2E_3}$ and $\mathrm{A_3C_3D_1E_2}$. After obtaining these combinations, we utilised generalised linear regression to build a reduced model for evaluating the classifier under different levels with various factors. The reduced model $\hat{\eta}(\mathrm{A_i}, \mathrm{C_j}, \mathrm{D_m}, \mathrm{E_n})$ is

expressed as Equation ((12)):

$$\hat{\eta}(A_i, C_j, D_m, E_n) = \bar{\eta}_{A_i,C_j} + \bar{\eta}_{A_i,D_m} + \bar{\eta}_{A_i,E_n} - 2\bar{\eta}_{A_i}, \quad \text{where} \quad i, j, m \text{ and } n{=}1, 2, 3. \tag{12}$$

where $\bar{\eta}_A$ is the mean of S/N_{LTB} under "factor A with i level," $\bar{\eta}_{AC}$ is the mean of S/N under the interaction of "factor A with i level" and "factor C with j level," and so on. After R-square testing of the reduced model ($\hat{\eta}$), the results show that R^2= 98.39%, R^2_{Adj}= 93%, PRESS (Prediction Error Sum of Squares)= 10.78, and R^2_{Pred}= 67.31%. Therefore, the reduced model is statistically proven to predict the S/N_{LTB} of response for the combinations of factors and level settings.

Comparing with the combinations of $A_1C_3D_2E_3$ and $A_3C_3D_1E_2$ from the reduced model, we evaluated which is a robust combination of classifier, by the S/N_{LTB} (refer to Equation (12)), the detection accuracy of classifier (ACC, refer to Table 2 and Table B-1 in Appendix B.3) and Kolmogorov-Smirnov (KS) value (refer to Appendix C: Equation (C.3)). The larger of S/R_{LTB}, ACC and KS, the better performance is. According to the Figure 6, the blue points of Case 1 ($A_1C_3D_2E_3$) and Case 2 ($A_3C_3D_1E_2$) were all located on the better detection boundary. The blue points were the samples, and the red line was a boundary line of random guesses. "Case 1" was uniform distributed on False Positive Rate (FPR, refer to Appendix C: Equation (C.2)) from 0.2 to 0.4, but "Case 2" was uniform distributed on True Positive Rate (TPR, refer to Appendix C: Equation (C.1)) from 0.6 to 0.85. In our identifying decision, we focused on more stable True Positive Rate than False Positive Rate, so that the final robust classifier was under the combination of $A_3C_3D_1E_2$ no matter whether from the R-square statistics or the performance (ACC and KS) in ROC space by statistics in Figure 6 and Table 5.

Case 2 of the first approach used binary fifth order nonlinear regression model where detection accuracy (ACC) was 81.22% and was better than the lower order term of Case 1. Therefore, the final classifier following the robust

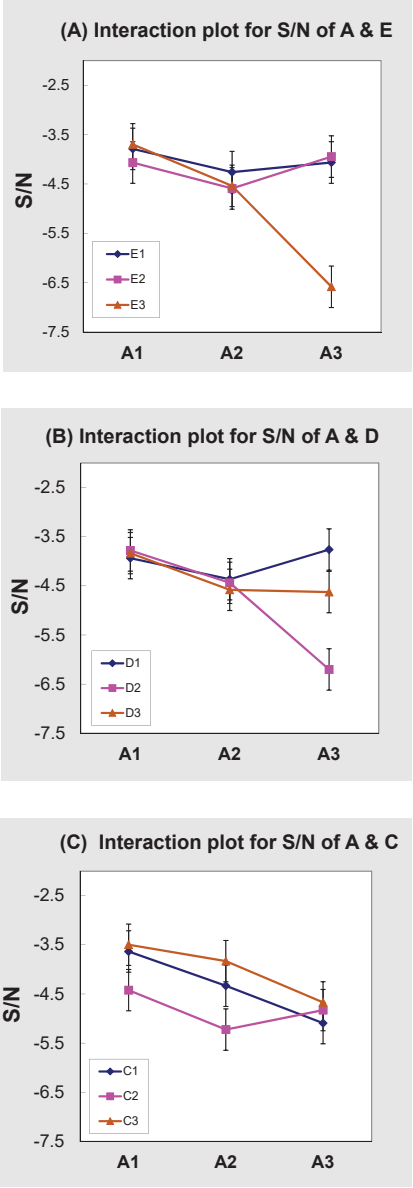

Figure 5: Interaction plots for S/N.

Table 5: Evaluating two classifiers with S/R_{LTB}, detection accuracy (ACC) of classifier and Kolmogorov-Smirnov (KS) value.

Case	Classifier	S/R_{LTB} (dB)	ACC (%)	KS
1.($A_1C_3D_2E_3$)	$\hat{Z} = X^4 \cdot \beta \cdot Y^4 + \hat{\varphi}$	-3.27 dB	68.79 %	0.78
2.($A_3C_3D_1E_2$)	$\hat{Z} = X^5 \cdot \beta \cdot Y^5 + \hat{\varphi}$	-2.65 dB	81.22 %	0.86

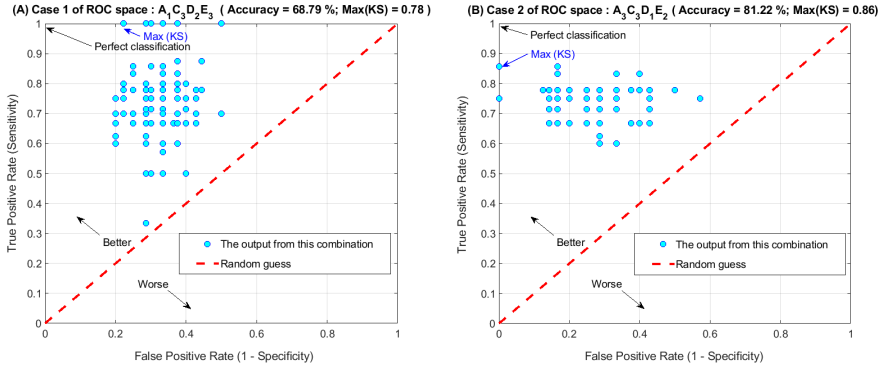

Figure 6: The distribution of receiver operating characteristic (ROC) space under the optimal condition of (A) Case 1: $A_1C_3D_2E_3$; (B) Case 2: $A_3C_3D_1E_2$.

parameter design ($A_3C_3D_1E_2$) is shown as Equation (13).

$$\hat{\mathbf{Z}} = \mathbf{X}^5 \cdot \boldsymbol{\beta} \cdot \mathbf{Y}^5 + \hat{\boldsymbol{\varphi}},$$

$$\text{and} \quad \hat{T}_{pr} = \widetilde{f}(\hat{\varphi}, DT_3) = \begin{cases} 1, & \hat{T} \in \text{OR3}, \quad \hat{\boldsymbol{\varphi}} \leqslant DT_3, \quad DT_3 = 0.04, \\ 0, & \hat{T} \in \text{Non-OR3}, \quad \hat{\boldsymbol{\varphi}} > DT_3, \quad DT_3 = 0.03, \end{cases} \tag{13}$$

5 Second approach: Radial Basis Function Neural Network (RBFNN)

The second approach consists of the classifier, curve fitting by RBFNN, and feature selection by GA to find the optimising parameters of the classifier.

This approach requires extensive computation when adjusting the weighting values and bias during each iteration and achieving a global optimum by GA. For this reason, we decided to build the classifier in the second approach under the final parameter design of only Factors A and C (Case 2: A_3C_3), because Factors D and E are the parameters of building the PR.

5.1 Classifier

The classifier is made by RBFNN, and the transform function is Gaussian function, which is called Radiated Basic Function (RBF) in Matlab Toolbox [23] is expressed as

$$\begin{aligned} &\phi(n) = \text{radbas}(n) = \exp(-n^2), \\ &\text{where} \quad n = \|\omega_1 - \mathbf{Z}\| \cdot b_1; \quad b_1 = -0.8326/\text{SC}, \end{aligned} \tag{14}$$

where ω_1 is the weighting value of the hidden layer; $\mathbf{Z} = \text{N}(\mathbf{SNR})$ is the input data; b is the bias of the hidden layer; SC is spread constant and is like the variance of Gaussian function. The value 0.8326 is defined as the net input being $\sqrt{}(-\log(0.5)$ or 0.8326) when RBF=0.5. The setting of SC is sensitive for determining if the network is overfitting or under-fitting, so it will be optimised by GA in subsection 5.2.

Since RBF is a continuous function but the original target (T) is categorical, it needs to convert the categorical variables to continuous variables by Omega transform ($\text{f}(\text{T})$) [35, 36, 38], which is

$$T_{nn} = \text{f}(\text{T}) = 10 \cdot \log_{10}\left(\frac{\text{T}}{1-\text{T}}\right)\begin{cases} +\infty, & \text{T=1}, \quad \text{Target} \in \text{OR3}, \\ -\infty, & \text{T=0}, \quad \text{Target} \in \text{Non-OR3}. \end{cases} \tag{15}$$

Therefore, RBFNN can calculated from Equation (14) and Equation (15), which is given as

$$\begin{aligned} &\hat{\text{T}} = \textstyle\sum_{\iota=1}^{h} \omega_{2,\iota} \cdot \phi_\iota + b_{2,\iota}, \\ &\quad \text{where} \quad \omega_{2,\iota} = \frac{\phi_\iota^T \cdot T_{nn}}{\phi_\iota^T \cdot \phi_\iota}; \quad b_{2,\iota} = \frac{(\omega_{2,\iota})^2 \cdot \phi_\iota^T \cdot \phi_\iota}{T_{nn}^T \cdot T_{nn}}; \end{aligned} \tag{16}$$

where $\omega_{2,\iota}$ is the weighting value of the linear layer; $b_{2,\iota}$ is the bias of the linear layer; $\hat{T}$ is the output from RBFNN; ι=1,2,...,h; h is the number index of the hidden layer.

Since the output layer of RBFNN is linear, it is given from the Orthogonal Least Squares (OLS) learning algorithm [22]. To make the computation in each iteration more efficient in OLS, setting a tolerance ("Goal" in Matlab toolbox, refer to Equation (17)) is a strategy to balance the accuracy and the complexity of the final network. The setting of Goal also should be optimised by GA.

$$1 - \sum_{\iota=1}^{h} b_{2,\iota} < \text{Goal}, \tag{17}$$

After training from RBFNN, the predicting target ($\hat{T}$) should be transferred through the inverse omega transform ($f^{-1}(\hat{T})$) and the final target ($\hat{T}_{nn}$),

$$\hat{T}_{nn} = f^{-1}(\hat{T}) = \begin{cases} 1, & \hat{T} \approx +\infty, \quad \text{Target} \in \text{OR3}, \\ 0, & \hat{T} \approx -\infty, \quad \text{Target} \in \text{Non-OR3}. \end{cases} \tag{18}$$

5.2 Feature selection

The feature selection is finding the global optimum of "SC" and "Goal" in RBFNN by GA. The algorithm of GA utilises Matlab toolbox. The Genetic parameters are set as Population size = 100; Crossover rate = 0.8; and Generations = 50. The objective function (Equation (19)), which is under the range limitation of SD and Goal, is calculated by the square root of the mean of each R^2 and R^2_{pred}, which is from Equation (C.4) and Equation (C.6) (refer to Appendix C), through Leave-One-Out Cross Validation (LOOCV) [26, 39].

$$\nu = \sqrt{\frac{\sum_{p=1}^{\hat{n}} R^2_{(p)}}{\hat{n}} \cdot \frac{\sum_{p=1}^{\hat{n}} R^2_{Pred(p)}}{\hat{n}}}, \tag{19}$$
$$\text{where} \quad \hat{n} = 101; 1 < SC < 1000; \quad 0.01 < \text{Goal} < 0.1.$$

6 Results and Discussion

From the final parameter design of the first approach, the results show that Factor A at Level 3, the features extracted from HF, better expressed the characteristics of acoustic signatures than those from occurrence frequency (OF). Factor C at Level 3 means that SNR was more sensitive to the distribution of frequency and pressure terms. In accordance with the final combination of factors, the performance of the first approach and the second approach were compared (refer to Figure 7 and Table 6).

Figure 7(A) shows the three-dimensional SNR distribution under optimal conditions (A_3C_3). Figure 7(B) displays the normalised SNR of PR model from Equation (13). Figure 7(C) displays the normalised SNR of RBFNN model. Table 6 shows the results after evaluating the two approaches with detection accuracy (ACC) and the confusion matrix of ROC (refer to Table 2) under training, validating and testing processes. The larger ACC (TP and TN) is and the smaller FP and FN are, the better the performance is.

The first approach consisted of PR classifier and a reduced model (proposed in this paper and referred to as PR model), which used the Taguchi method and ANOVA. The training accuracy was 81.9% (664 samples), the validating accuracy was 82.76% (58 samples) and the testing accuracy was higher than RBFNN and up to 81.03% (58 samples), which was calculated using only 273 seconds for training and about 3.8 seconds for predicting.

The second approach used RBFNN, and it optimised the classifier parameters by GA (Goal = 0.4891 and SC = 1). Figure 7 and Table 6 show that RBFNN displays better curve-fitting than PR model with R test, R^2 test, and ACC. As the data samples in different voyages are not same (refer to Table 1), we distributed the training and validating samples between the PR approach and RBFNN based on the ratio of each voyage to avoid too much overfitting. The training accuracy was 85.5% (200 samples) and the validating accuracy was 70% (40 samples), where training and validating samples were lower than PR classifier, but testing accuracy still could reach 62.48% (540 samples).

Table 6: Evaluating two approaches (PR approach($A_3C_3D_1E_2$) and RBFNN approach (A_3C_3)) by detection accuracy (ACC, %) and the confusion matrix under training, validating and testing process.

(A) PR (train) : ACC = 81.9 %

	T=1	T=0
$\hat{T}$=1	TP = 251	FP = 39
$\hat{T}$=0	FN = 81	TN = 293
Total samples	332	332
Elapsed time	273 seconds	

(B) RBFNN (train) : ACC = 85.5 %

	T=1	T=0
$\hat{T}$=1	TP = 82	FP = 11
$\hat{T}$=0	FN = 18	TN = 89
Total samples	100	100
Elapsed time	16197 seconds	

(C) PR (validate) : ACC = 82.76 %

	T=1	T=0
$\hat{T}$=1	TP = 23	FP = 4
$\hat{T}$=0	FN = 6	TN = 25
Total samples	29	29
Elapsed time	3.5 seconds	

(D) RBFNN (validate) : ACC = 70 %

	T=1	T=0
$\hat{T}$=1	TP = 14	FP = 6
$\hat{T}$=0	FN = 6	TN = 14
Total samples	20	20
Elapsed time	0.1 seconds	

(E) PR (test) : ACC = 81.03 %

	T=1	T=0
$\hat{T}$=1	TP = 22	FP = 3
$\hat{T}$=0	FN = 8	TN = 25
Total samples	29	29
Elapsed time	3.8 seconds	

(F) RBFNN (test) : ACC = 64.6 %

	T=1	T=0
$\hat{T}$=1	TP = 159	FP = 80
$\hat{T}$=0	FN = 111	TN = 190
Total samples	270	270
Elapsed time	0.1 seconds	

Although the predicting time was 30 times faster than the PR classifier, the training time was 59 times higher for building the model.

Although the training performance of R-square testing and accuracy of RBFNN model displayed better fitting than PR model, it included the noise (the peak values in Figure 7 (A.1) and (C.1)) and led to worse performance on the prediction of OR3. Since the Non-OR3 samples included the ambient noise in Figure 7 (A.2) and the RBFNN model approached the noise in Figure 7 (C.2) well, the performance of Non-OR3 RBFNN works better than the performance of OR3 in Table 6 (B) and (F).

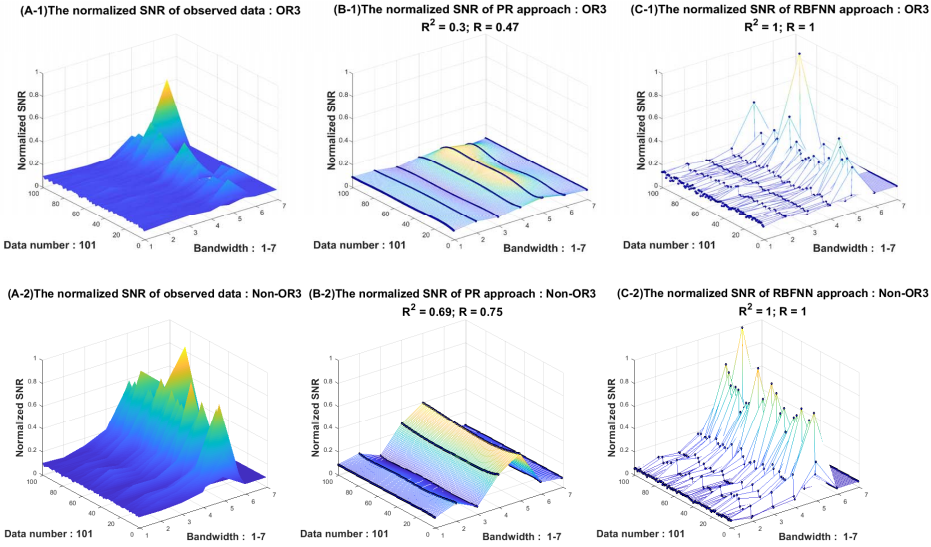

Figure 7: (A) The SNR data; (B) the normalised SNR of PR approach under the optimal condition ($A_3C_3D_1E_2$); (C) the normalised SNR of RBFNN approach under the optimal condition (A_3C_3) of Model 1 (OR3) and Model 0 (Non-OR3).

Since the target of the identification system is specific for OR3 and the first approach significantly reduces the computational time (when training the classifier and feature selection) while enhancing the classification accuracy, the overall performance of the automatic identification system includes the prediction and the accuracy. Thus, the PR model proposed in this paper has better performance than the RBFNN model. The results show that the feature extraction of OT and HT and that the SNR of the FF and its PSD is appropriate for our identification system.

7 Conclusion

We developed Automatic Identification System for Vehicles using Acoustic Signature (AIS4VAS), which is composed of feature extraction, classification algorithms, and feature selection, to perform the identification of noises that will identify a specific ship. This research utilises signal processing to extract the essential features of the acoustic signature from a bottom mounted hydrophone. We utilised factor analysis to describe variability and interaction among observed acoustic signatures in feature selection.

The final combination of factors describe the SNR under interaction with frequency and its PSD, which could increase the contribution of harmonic signal characteristics. The classifier constructed by PR, which is made by HF features from unmasking the frequency BW of OR3 shipping noises, is superior to that of the RBFNN model. Last but not least, results suggest that feature extraction works better for our targets and identification system.

Appendices

A Feature extraction

A.1 Derivatives of extracting the FF

Φ(t) is raw data from the hydrophone, after which STFT can get the acoustic pressure value P[t, F], where t is 3-minute long data. Filtering the low frequency and high frequency noise for each minute of data results in the filtering pressure value $\widetilde{\mathsf{P}}[\mathsf{t}, \widetilde{\mathsf{F}}]$. We extract and normalise the peak pressure from filtering values $\widetilde{\mathsf{P}}[\mathsf{t}, \widetilde{\mathsf{F}}_{\mathsf{BW_k}}]$ under each BW to get $\mathsf{N_s}(\widetilde{\mathsf{P}})$, where t is still a 3-minute long data set, $\mathsf{F}_{\mathsf{BW_k}}$ is the frequency range under each BW, and k

is the index number of BW from 1 to 7. The normalisation formula is used to bring all values into the range [0,1] and is called unity-based normalisation, which is expressed as

$$N_s(\widetilde{P}) \equiv N(\widetilde{P}_s) := (\widetilde{P}_s - \widetilde{P}_{min})/(\widetilde{P}_{max} - \widetilde{P}_{min}), \tag{A.1}$$

where s is the index of $\widetilde{P}$. Calculating the marginal probability density function (MPDF) of $N(\widetilde{P})$ to get $\breve{P}[t, \breve{F}_{BW_k}]$ is

$$\breve{P}_s[t, \breve{F}_{BW_k}] = \text{MPDF}(\widetilde{P}_s) := N_s(\widetilde{P}) / \sum_t N_t(\widetilde{P}) \ \text{, t is the index number of N.} \tag{A.2}$$

We only extract the peak pressure value from 95% of total energy to be "the pressure of fundamental frequency" $\hat{P}[t, \hat{F}_{BW_k}]$ (Equation A.3), where w is the index number of selecting 95 % peaks under each BW. Calculating the 95% of total energy is a kind of second filter to process the next procedure.

$$\hat{\mathbf{P}} = [\breve{P}_1 \quad \breve{P}_2 \quad ... \quad \breve{P}_w]' := \{\breve{P}_s | \sum_{s=1}^{w} \breve{P}_s[t, \breve{F}_{BW_k}] \leqslant 0.95, \quad \breve{P}_1 > \breve{P}_2 > ... > \breve{P}_w\}. \tag{A.3}$$

$$FF = \hat{\mathbf{F}} = [\hat{F}_1 \quad \hat{F}_2 \quad ... \quad \hat{F}_w]' := \{\hat{F}_w | \hat{F}_w \in \hat{F}_{BW_k}, \quad k = 1, 2, ..., 7\}. \tag{A.4}$$

The FF ($\hat{\mathbf{F}}$) are defined as the frequencies under each BW ($\hat{F}_{BW_k}$), and they are a subset of "the pressure of fundamental frequency ($\hat{\mathbf{P}}$)".

A.2 Examples of calculating OT, HT and their correlation

Table A-1 is an example of calculating the OT and HT. There are 4 samples and 6 different frequencies of Occurrence Frequency (OF). Here, Harmonic Frequencies were 11 Hz, 22 Hz, 44 Hz, and 66 Hz. OTs at 11 Hz appear 4

times, and, at 22Hz, they appear 3 times within these 4 samples, and so on. Harmonic Times at 22 Hz occur 2 times, including 44 Hz and 66 Hz.

We randomly chose 32 from 332 (OR3 target) to be a training sample (Table 6 (A)) and repeated the probability of selection until the total number of samples reached 101 sets. We followed the above procedure to get OT and HT from each set. Since HT is calculated from OT, we analyse the correlation of OT and HT at different BWs first. From Figure A.1, we see that HT is highly negatively correlated to the BW and OT is moderately negatively correlated with BW4 (250-499 Hz band) and BW7 (1k-2k Hz band). Because of the low frequency band of ambient noise interference, there is no correlation between OT and HT and the frequency index and OT are below 250 Hz. This shows that HT is highly correlated with OT only at and above the 250 Hz band.

Table A-1: Examples of calculating Occurrence Times and Harmonic Times.

Occurrence Freq.	11 Hz	15 Hz	22 Hz	37 Hz	44 Hz	66 Hz
Harmonic Freq.	11 Hz		22 Hz		44 Hz	66 Hz
Sample (1)	√	√	√	√		√
Sample (2)	√		√	√	√	
Sample (3)	√	√		√	√	√
Sample (4)	√	√		√		
Occurrence Times	4	3	2	4	2	2
Harmonic Times	4	1	3	1	1	1

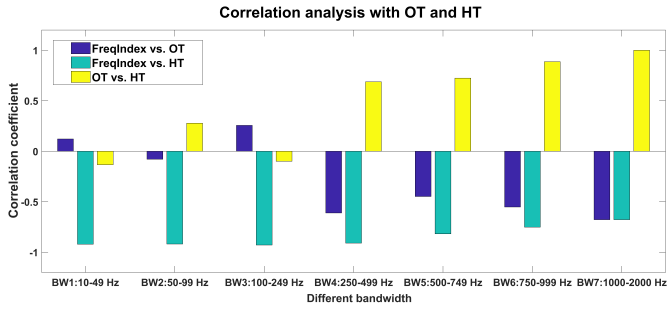

Figure A.1: Correlation analysis of Occurrence Times and Harmonic Times.

A.3 Example of extracting MF from experimental data

Figure A.2 shows how to extract MF by procedure of feature extraction (Figure 4) and the PSD of OR3 from the aforementioned experiments (Table 1). The distribution of PSD from ocean cruising data is shown in Figure A.2(A-C). The audio data from December 2016 recorded more wind-dependent bubble and spray noise, which was caused by the worse sea state at that time. Due to heavy traffic near Kaohsiung harbour, the data quality from the Kaohsiung offshore test suffered interference from local commercial shipping noise. From (B-C), there were insignificant harmonic peaks because the PSD under 200 Hz fluctuated with the nearby shipping noise and the closest point of approach (CPA) or the water depth was greater than in other experiments. With larger distribution on PSD between 400 Hz to 900 Hz, its noise level fluctuated with wind-dependent bubble and spray noise (Figure A.2 (B)). The obvious harmonic peak in Figure A.2(D) was due to the small CPA during the harbour testing, resulting in the recording sound pressure level being louder and clearer. Figure A.2(E) was expressed that how to extract the main frequency and three examples of the harmonic frequency of generators (red and green) and main engine (blue). Many factors impacted extracting main frequency (MF) from frequency band by signal processing and feature extraction. Nevertheless, the procedure in this paper was not to extract frequency features from a noise masking band. The procedure was to quantise the frequency features distribution within each BW by the signal to noise ratio (SNR).

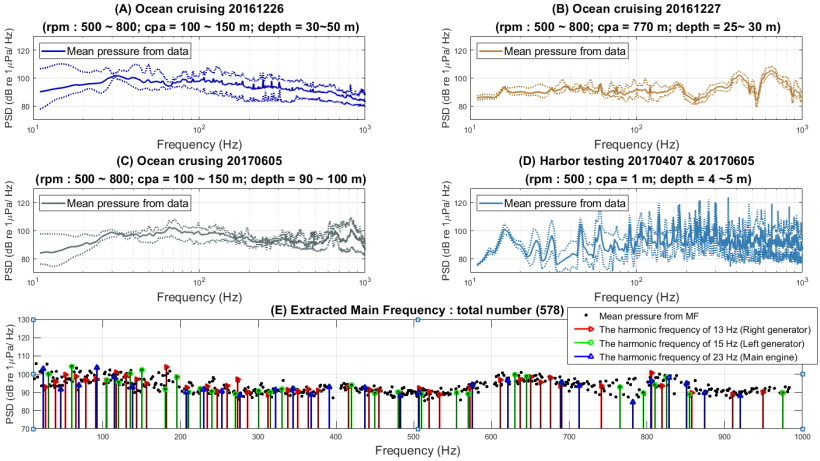

Figure A.2: The distribution of power spectral density of OR3 from (A-C) ocean cruising data; (D) harbour testing data; (In (A-D), the solid line is mean PSD value and the dotted lines are the higher bound and lower bound of PSD); (E) extracting the main frequency and harmonic frequency from whole experimental data.

B First approach

B.1 Derivatives of Polynomial Regression (PR)

The first step in curve fitting is building the polynomial of YZ plane under seven BW. Y plane ($\mathbf{y}$) is made by the training sets size, which is 101 in this paper. For each BW, the regression output of 101 sets is

$$\mathbf{z}_{\mathrm{p}\cdot 1} = \mathbf{y}_{\mathrm{p}\cdot \mathrm{r}}\boldsymbol{\alpha}_{\mathrm{r}\cdot 1} + \boldsymbol{\varepsilon}_{\mathrm{p}\cdot 1}, \quad \mathrm{p} = 1, 2, ..., 101, \quad \mathrm{r} = 0, 1, 2, ..., \mathrm{O}_{\mathrm{YZ}}. \tag{B.1}$$

where $\mathbf{z}$ is the predicted output from the regression, r is the setting value of power from YZ plane, p is the index number of training sets, $\boldsymbol{\alpha}$ is the matrix

of coefficient estimates for observation, and O_{YZ} is one of the controllable factors from Table 3. The residual of regression term $\boldsymbol{\varepsilon}$ is expressed as

$$\boldsymbol{\varepsilon} = \boldsymbol{z} - \boldsymbol{y} \cdot \boldsymbol{\alpha}. \tag{B.2}$$

Calculating the square of residual ($\mathbf{L}$) is expressed as

$$\mathbf{L} = \boldsymbol{\varepsilon}'\boldsymbol{\varepsilon} = (\boldsymbol{z} - \boldsymbol{y}\boldsymbol{\alpha})'(\boldsymbol{z} - \boldsymbol{y}\boldsymbol{\alpha}) = \boldsymbol{z}'\boldsymbol{z} - 2\boldsymbol{\alpha}'\boldsymbol{y}'\boldsymbol{z} + \boldsymbol{\alpha}'\boldsymbol{y}'\boldsymbol{y}\boldsymbol{\alpha}, \tag{B.3}$$

Get the objective function from Equation (B.3)

$$\text{Min } \mathbf{L} = \sum_{ii=1}^{n} \varepsilon_{ii}^2 \Rightarrow \frac{\partial \mathbf{L}}{\partial \boldsymbol{\alpha}} = -2\boldsymbol{y}'\boldsymbol{z} + 2\boldsymbol{y}'\boldsymbol{y}\boldsymbol{\alpha} = 0, \tag{B.4}$$

where ii is the index number of $\boldsymbol{\varepsilon}$.

Solving the simultaneous equations, we obtain the coefficient matrix $\boldsymbol{\alpha}$

$$\boldsymbol{\alpha} = (\boldsymbol{y}'\boldsymbol{y})^{-1}\boldsymbol{y}'\boldsymbol{z}. \tag{B.5}$$

Repeating the above procedures for each BW, we can get the whole regression equation of seven BWs, which is expressed as Equation (B.6), where k is the number of BWs

$$\begin{gathered} \hat{\boldsymbol{Z}}_k = \boldsymbol{\alpha}_{k,r} \cdot \boldsymbol{Y}^r + \boldsymbol{\varphi}_k, \quad k = 1, 2, ..., 7. \\ \hat{\boldsymbol{Z}}_k = [\boldsymbol{z}_1 \quad \boldsymbol{z}_2 \quad ... \quad \boldsymbol{z}_k]', \quad \boldsymbol{Y}^r = [\boldsymbol{y}^0 \quad \boldsymbol{y}^1 \quad ... \quad \boldsymbol{y}^r]', \end{gathered} \tag{B.6}$$

$$\text{where } \boldsymbol{\alpha}_{k,r} = \boldsymbol{\Lambda}_r \Rightarrow \begin{bmatrix} \alpha_{1,0} & \alpha_{1,1} & ... & \alpha_{1,r} \\ \alpha_{2,0} & \alpha_{2,1} & ... & \alpha_{2,r} \\ \vdots & \vdots & \vdots & \vdots \\ \alpha_{k,0} & \alpha_{k,1} & ... & \alpha_{k,r} \end{bmatrix}_{k \cdot r} = \begin{bmatrix} \Lambda_1 \\ \Lambda_2 \\ \vdots \\ \Lambda_r \end{bmatrix} \tag{B.7}$$

The second step is regression of the coefficient matrix of YZ plane (Equation (B.7)), as well as X plane, which is also made from seven BWs

$$\boldsymbol{\Lambda}_{r \cdot 1} = \boldsymbol{X}_{r \cdot d}^{d} \boldsymbol{\beta}_{d \cdot 1} + \hat{\boldsymbol{\varepsilon}}_{r \cdot 1}, \quad d = 0, 1, 2, ..., O_{X\Lambda}. \tag{B.8}$$

where β is the matrix of coefficient estimates for a multilinear regression on X plane, $\mathbf{d}$ is the setting value of power of building X plane and coefficient matrix $\boldsymbol{\alpha}$, $\hat{\boldsymbol{\varepsilon}}$ is the residual term, and $\mathsf{O}_{\mathsf{X}\Lambda}$ is one of the controllable factors from Table 3. Combining Equation (B.6) and Equation (B.8), one can obtain Equation (B.9). Equation (B.10) is the residual, which is the observed deducted from the predicted value.

$$\hat{\mathbf{Z}}_{\mathbf{k}} = \boldsymbol{\Lambda}_{\mathbf{r}} \cdot \boldsymbol{Y}^{\mathrm{r}} + \boldsymbol{\varphi}_{\mathrm{k}} = (\mathbf{X}^{\mathrm{d}}_{\mathrm{r}\cdot\mathrm{d}}\boldsymbol{\beta}_{\mathrm{d}\cdot 1} + \hat{\boldsymbol{\varepsilon}}_{\mathbf{r}\cdot\mathbf{1}}) \cdot \boldsymbol{Y}^{\mathrm{r}} + \boldsymbol{\varphi}_{\mathrm{k}} = \mathbf{X}^{\mathrm{d}} \cdot \boldsymbol{\beta} \cdot \boldsymbol{Y}^{\mathrm{r}} + \hat{\boldsymbol{\varphi}}_{\mathbf{k}}, \quad \text{(B.9)}$$

$$\hat{\boldsymbol{\varphi}}_{\mathbf{k}} = \boldsymbol{\varphi}_{\mathrm{k}} + \hat{\boldsymbol{\varepsilon}} \cdot \boldsymbol{Y}^{\mathrm{r}} = \mathbf{Z}_{\mathrm{data}} - \hat{\mathbf{Z}}_{\mathbf{k}}. \quad \text{(B.10)}$$

B.2 Experimental results table and ANOVA of $L_{27}(3^{13})$ in feature selection

Exp No.	A 1	B 2	AxB 3	AxB 4	C 5	AxC 6	AxC 7	D 8	AxD 9	AxD 10	E 11	AxE 12	AxE 13	S/N (LTB)
1	1	1	1	1	1	1	1	1	1	1	1	1	1	-3.429
2	1	1	1	1	2	2	2	2	2	2	2	2	2	-4.338
3	1	1	1	1	3	3	3	3	3	3	3	3	3	-3.099
4	1	2	2	2	1	1	1	2	2	2	3	3	3	-3.379
5	1	2	2	2	2	2	2	3	3	3	1	1	1	-4.312
6	1	2	2	2	3	3	3	1	1	1	2	2	2	-3.764
7	1	3	3	3	1	1	1	3	3	3	2	2	2	-4.095
8	1	3	3	3	2	2	2	1	1	1	3	3	3	-4.615
9	1	3	3	3	3	3	3	2	2	2	1	1	1	-3.625
10	2	1	2	3	1	2	3	1	2	3	1	2	3	-4.031
11	2	1	2	3	2	3	1	2	3	1	2	3	1	-5.326
12	2	1	2	3	3	1	2	3	1	2	3	1	2	-4.022
13	2	2	3	1	1	2	3	2	3	1	3	1	2	-4.515
14	2	2	3	1	2	3	1	3	1	2	1	2	3	-5.272
15	2	2	3	1	3	1	2	1	2	3	2	3	1	-3.995
16	2	3	1	2	1	2	3	3	1	2	2	3	1	-4.451
17	2	3	1	2	2	3	1	1	2	3	3	1	2	-5.075
18	2	3	1	2	3	1	2	2	3	1	1	2	3	-3.476
19	3	1	3	2	1	3	2	1	3	2	1	3	2	-3.261
20	3	1	3	2	2	1	3	2	1	3	2	1	3	-5.316
21	3	1	3	2	3	2	1	3	2	1	3	2	1	-6.221
22	3	2	1	3	1	3	2	2	1	3	3	2	1	-8.202
23	3	2	1	3	2	1	3	3	2	1	1	3	2	-3.845
24	3	2	1	3	3	2	1	1	3	2	2	1	3	-2.703
25	3	3	2	1	1	3	2	3	2	1	2	1	3	-3.817
26	3	3	2	1	2	1	3	1	3	2	3	2	1	-5.323
27	3	3	2	1	3	2	1	2	1	3	1	3	2	-5.088

Figure B.1: Experimental results (S/N_{LTB}) with five controllable factors in Table 3 for $L_{27}(3^{13})$ design.

B.3 Detection accuracy of PR for Case 1 and Case 2

Table B-1: A confusion matrix of ROC in classifier of (A) Case 1: $A_1C_3D_2E_3$ (B) Case 2: $A_3C_3D_1E_2$. (The definition of A, B and C factors refer to Table 3).

(A) Case 1 : ACC= 68.79 %

	T=1	T=0
$\hat{T}$=1	TP = 224	FP = 99
$\hat{T}$=0	FN = 108	TN = 233
Total samples	332	332

(B) Case 2 : ACC = 81.22 %

	T=1	T=0
$\hat{T}$=1	TP = 248	FP = 41
$\hat{T}$=0	FN = 84	TN = 291
Total samples	332	332

C Equations for diagnostic ability of classifier

True positive rate (TPR = sensitivity, SEN) and false positive rate (FPR = 1-specificity) are calculated from the confusion matrix, which is seen in Table 2 and Table B-1. From TPR and FPR, we can calculate the KS (Kolmogorov-Smirnov) test. The KS is made up of TPR and FPR. When KS is 1, the model attains perfect classification, which means the condition of sensitivity is 1 and specific = 1. The equations of TPR, FPR and KS are

$$\mathrm{TPR} = \mathrm{TP}/(\mathrm{TP} + \mathrm{FP}) = \mathrm{Sensitivity}, \tag{C.1}$$

$$\mathrm{FPR} = 1 - \mathrm{SPC} = 1 - [\mathrm{TN}/(\mathrm{TN} + \mathrm{FP})], \tag{C.2}$$

$$\mathrm{KS} = \mathrm{Max}(\mathrm{TPR} - \mathrm{FPR}). \tag{C.3}$$

The second method is evaluating the reduced model by calculating the coefficient of determination (R^2) [15, 26]. The quantity R-square (R^2) is defined as Equation (C.4), where SS_{Model} is the sum of square from the model and SS_{total} is the total sum of square value.The value of R-square must be within zero to one. The larger the value of R-square is, the more desirable it is. The adjusted R-square (R^2_{Adj}) from Equation (C.5) is a variation of the ordinary R-square as increasing or decreasing the number of model terms, where df_E

is degrees of freedom of the error term and df_{Total} is the total number of degrees of freedom. The larger the difference between R^2 and R^2_{Adj} is, the larger the residual of this model is. The predicted R-square (R^2_{Pred}) from Equation (C.6), which is based on PRESS, shows how well the model predicts the responses for new testing. PRESS stands for Prediction Error Sum of Squares and is given by cross validation, where T is the original target and $\hat{T}$ is the predicting target. The smaller PRESS is, the better the prediction is.

$$R^2 = \frac{SS_{Model}}{SS_{Total}} = 1 - \frac{SS_E}{SS_{Total}}, \tag{C.4}$$

$$R^2_{Adj} = 1 - \frac{SS_E/df_E}{SS_{Total}/df_{Total}}, \tag{C.5}$$

$$R^2_{Pred} = 1 - \frac{PRESS}{SS_{Total}}, \tag{C.6}$$

$$PRESS \approx \sum_{\ell=1}^{\xi} \left[T_\ell - \hat{T}_\ell \right]^2. \tag{C.7}$$

The third method is verification by correlation coefficient (R), which is a statistical method to denominate the relationship between two variables and is seen in Equation (C.8). $S_{\hat{Z}Z_{data}}$ is the covariance between model $\hat{Z}$ and data Z_{data}. $S_{\hat{Z}}$ is the standard deviation of model $\hat{Z}$, and $S_{Z_{data}}$ is the standard deviation of data Z_{data}.

$$R = S_{\hat{Z}Z_{data}}/(S_{\hat{Z}} \cdot S_{Z_{data}}). \tag{C.8}$$

References

[1] Nathan D Merchant, Kurt M Fristrup, Mark P Johnson, Peter L Tyack, Matthew J Witt, Philippe Blondel, and Susan E Parks. Measuring

acoustic habitats. *Methods in Ecology and Evolution*, 6(3):257–265, 2015. doi:10.1111/2041-210X.12330. C320

[2] Nathan D Merchant, Philippe Blondel, D Tom Dakin, and John Dorocicz. Averaging underwater noise levels for environmental assessment of shipping. *The Journal of the Acoustical Society of America*, 132(4):EL343–EL349, 2012. doi:10.1121/1.4754429. C320

[3] Chi-Fang Chen, Hsiang-Chih Chan, Ray-I Chang, Tswen-Yung Tang, Sen Jan, Chau-Chang Wang, Ruey-Chang Wei, Yiing-Jang Yang, Lien-Siang Chou, Tzay-Chyn Shin, et al. Data demonstrations on physical oceanography and underwater acoustics from the marine cable hosted observatory (macho). In *OCEANS, 2012-Yeosu*, pages 1–6. IEEE, 2012. doi:10.1109/OCEANS-Yeosu.2012.6263639. C320

[4] Sauda Sadaf P Yashaswini, Soumya Halagur, Fazil Khan, and Shanta Rangaswamy. A literature survey on ambient noise analysis for underwater acoustic signals. *International Journal of Computer Engineering and Sciences*, 1(7):1–9, 2015. doi:10.26472/ijces.v1i7.37. C321

[5] Shuguang Wang and Xiangyang Zeng. Robust underwater noise targets classification using auditory inspired time-frequency analysis. *Applied Acoustics*, 78:68–76, 2014. doi:10.1016/j.apacoust.2013.11.003. C321

[6] LG Weiss and TL Dixon. Wavelet-based denoising of underwater acoustic signals. *The Journal of the Acoustical Society of America*, 101(1):377–383, 1997. doi:10.1121/1.417983. C321

[7] Timothy Alexis Bodisco, Jason D'Netto, Neil Kelson, Jasmine Banks, Ross Hayward, and Tony Parker. Characterising an ecg signal using statistical modelling: a feasibility study. *ANZIAM Journal*, 55:32–46, 2014. doi:10.21914/anziamj.v55i0.7818. C321

[8] JosÃľ Ribeiro-Fonseca and LuÃŋs Correia. Identification of underwater acoustic noise. In *OCEANS'94.'Oceans Engineering for Today's Technology and Tomorrow's Preservation.'Proceedings*, volume 2, pages II/597–II/602 vol. 2. IEEE. C321, C327

[9] Linus YS Chiu and Hwei-Ruy Chen. Estimation and reduction of effects of sea surface reflection on underwater vertical channel. In *Underwater Technology Symposium (UT), 2013 IEEE International*, pages 1–8. IEEE, 2013. doi:10.1109/UT.2013.6519874. C321

[10] G.M. Wenz. *Acoustic ambient noise in the ocean: spectra and sources*. Thesis, 1962. doi:10.1121/1.1909155. C321

[11] Donald Ross. *Mechanics of underwater noise*. Elsevier, 2013. doi:10.1121/1.398685. C321

[12] Chris Drummond and Robert C Holte. Exploiting the cost (in) sensitivity of decision tree splitting criteria. In *ICML*, volume 1, 2000. C322

[13] Charles Elkan. The foundations of cost-sensitive learning. In *International joint conference on artificial intelligence*, volume 17, pages 973–978. Lawrence Erlbaum Associates Ltd, 2001. C322

[14] Chris Gillard, Alexei Kouzoubov, Simon Lourey, Alice von Trojan, Binh Nguyen, Shane Wood, and Jimmy Wang. Automatic classification of active sonar echoes for improved target identification. C322

[15] Douglas C Montgomery. *Design and analysis of experiments*. John wiley & sons, 2017. doi:10.1002/9781118147634. C322, C350

[16] G Taguchi. Off-line and on-line quality control systems. In *Proceedings of International Conference on Quality Control*, 1978. C323, C333

[17] Sheng-Ju Wu, Sheau-Wen Shiah, and Wei-Lung Yu. Parametric analysis of proton exchange membrane fuel cell performance by using the taguchi

method and a neural network. *Renewable Energy*, 34(1):135–144, 2009. doi:10.1016/j.renene.2008.03.006. C323

[18] Genichi Taguchi. Introduction to quality engineering: designing quality into products and processes. Technical report, 1986. doi:10.1002/qre.4680040216. C323

[19] Richard Horvath, Gyula Matyasi, and Agota Dregelyi-Kiss. Optimization of machining parameters for fine turning operations based on the response surface method. *ANZIAM Journal*, 55:250–265, 2014. doi:10.21914/anziamj.v55i0.7865.

[20] Chuan-Tien Li, Sheng-Ju Wu, and Wei-Lung Yu. Parameter design on the multi-objectives of pem fuel cell stack using an adaptive neuro-fuzzy inference system and genetic algorithms. *International Journal of Hydrogen Energy*, 39(9):4502–4515, 2014. doi:10.1016/j.ijhydene.2014.01.034. C323

[21] Antoine Guisan, Thomas C Edwards Jr, and Trevor Hastie. Generalized linear and generalized additive models in studies of species distributions: setting the scene. *Ecological modelling*, 157(2-3):89–100, 2002. doi:10.1016/S0304-3800(02)00204-1. C323

[22] Sheng Chen, Colin FN Cowan, and Peter M Grant. Orthogonal least squares learning algorithm for radial basis function networks. *IEEE Transactions on neural networks*, 2(2):302–309, 1991. doi:10.1109/72.80341. C323, C339

[23] Howard Demuth and Mark Beale. Neural network toolbox for use with matlab-user's guide verion 4.0. 1993. C323, C338

[24] Janice Gaffney, Charles Pearce, and David Green. Binary versus real coding for genetic algorithms: A false dichotomy? *ANZIAM Journal*, 51:347–359, 2010. doi:10.21914/anziamj.v51i0.2776. C323

[25] Daniel May and Muttucumaru Sivakumar. Techniques for predicting total phosphorus in urban stormwater runoff at unmonitored

catchments. *ANZIAM Journal*, 45:296–309, 2004. doi:10.21914/anziamj.v45i0.889. C324

[26] Chang-Xue Jack Feng, Zhi-Guang Yu, and Andrew Kusiak. Selection and validation of predictive regression and neural network models based on designed experiments. *IIE Transactions*, 38(1):13–23, 2006. doi:10.1080/07408170500346378. C324, C339, C350

[27] Yin-Ying Fang, Ping-Jung Sung, Kai-An Cheng, Meng Fan Tsai, and Chifang Chen. Underwater radiated noise measurement of ocean researcher 3. In *The 29th Taiwan Society of Naval Architects and Marine Engineers Conference*, 2017. C324

[28] Yin-Ying Fang, Chi-Fang Chen, and Sheng-Ju Wu. Analysis of vibration and underwater radiated noise of ocean researcher 3. In *The 30th Taiwan Society of Naval Architects and Marine Engineers Conference*, 2018. C324

[29] Det Norske Veritas. Rules for classification of ships new buildings– special equipment and systems additional class– part 6 chapter 24– silent class notation. *Rules for Classification of Ships–Newbuildings*, 2010. C324, C325

[30] Underwater acoustics–quantities and procedures for description and measurement of underwater sound from ships-part 1–requirements for precision measurements in deep water used for comparison purposes. (ISO 17208-1:2012), 2012. C324, C325

[31] Bureau Veritas. Underwater radiated noise, rule note nr 614 dt r00 e. *Bureau Veritas*, 2014. C324

[32] R.J. Urick. *Principles of underwater sound*, volume 3. McGraw-Hill New York, 1983. C327

[33] Lars Burgstahler and Martin Neubauer. New modifications of the exponential moving average algorithm for bandwidth estimation. In *Proc. of the 15th ITC Specialist Seminar*, 2002. C327

[34] Bishnu Prasad Lamichhane. Removing a mixture of gaussian and impulsive noise using the total variation functional and split bregman iterative method. *ANZIAM Journal*, 56:52–67, 2015. doi:10.21914/anziamj.v56i0.9316. C327

[35] Chao-Ton Su. *Quality engineering: off-line methods and applications*. CRC press, 2016. C338

[36] Jiju Antony and Mike Kaye. *Experimental quality: a strategic approach to achieve and improve quality*. Springer Science & Business Media, 2012. C338

[37] Özkan Küçük, Tayeb Elfarah, Serkan Islak, and Cihan Özorak. Optimization by using taguchi method of the production of magnesium-matrix carbide reinforced composites by powder metallurgy method. *Metals*, 7(9):352, 2017. doi:10.3390/met7090352.

[38] G Taguchi. System of experimental design, quality resources. *New York*, 108, 1987. C338

[39] Gavin C Cawley and Nicola LC Talbot. Efficient leave-one-out cross-validation of kernel fisher discriminant classifiers. *Pattern Recognition*, 36(11):2585–2592, 2003. doi:10.1016/S0031-3203(03)00136-5. C339

Author addresses

1. **Y.-Y. Fang**, Department of Engineering Science and Ocean Engineering, National Taiwan University, Taipei 10617, Taiwan. mailto:d00525007@ntu.edu.tw

2. **C.-F. Chen**, Department of Engineering Science and Ocean Engineering, National Taiwan University, Taipei 10617, Taiwan. mailto:chifang@ntu.edu.tw

3. **S.-J. Wu**, [1]Department of Power Vehicle and Systems Engineering, Chung Cheng Institute of Technology, National Defense University, Tauyuan City 33551, Taiwan. [2]System Engineering and Technology Program, National Chiao Tung University, Hsinchu City 30010, Taiwan
mailto:wusj44@gmail.com